THE JOURNAL OF BIOLOGICAL CHEMISTRY VOL. 288, NO. 8, pp. 5694–5706, February 22, 2013

Specific Conserved C-terminal Amino Acids of *Caenorhabditis elegans* HMP-1/α-Catenin Modulate F-actin Binding Independently of Vinculin*[S]

Received for publication, November 19, 2012 Published, JBC Papers in Press, December 27, 2012, DOI 10.1074/jbc.M112.438093

Stephanie L. Maiden[‡§1], Neale Harrison[¶2], Jack Keegan[‡], Brian Cain[‡], Allison M. Lynch[‡], Jonathan Pettitt[¶], and Jeff Hardin[‡§3]

From the [‡]Department of Zoology and the [§]Molecular and Cellular Pharmacology Program, University of Wisconsin, Madison, Wisconsin 53706 and the [¶]School of Medical Sciences, Institute of Medical Sciences, University of Aberdeen, Aberdeen AB25 2ZD, United Kingdom

Background: α-Catenin is a crucial link between adherens junctions and F-actin.
Results: C-terminal amino acids in HMP-1/α-catenin quantitatively modulate its ability to bind F-actin, but a putative vinculin-binding domain is not required *in vivo*.
Conclusion: Key C-terminal residues in α-catenin modulate its ability to bind F-actin.
Significance: This is the first genetic dissection of the ability of α-catenin to bind F-actin.

Stable intercellular adhesions formed through the cadherin-catenin complex are important determinants of proper tissue architecture and help maintain tissue integrity during morphogenetic movements in developing embryos. A key regulator of this stability is α-catenin, which connects the cadherin-catenin complex to the actin cytoskeleton. Although the C-terminal F-actin-binding domain of α-catenin has been shown to be crucial for its function, a more detailed *in vivo* analysis of discrete regions and residues required for actin binding has not been performed. Using *Caenorhabditis elegans* as a model system, we have characterized mutations in *hmp-1*/α-catenin that identify HMP-1 residues 687–742 and 826–927, as well as amino acid 802, as critical to the localization of junctional proximal actin during epidermal morphogenesis. We also find that the S823F transition in a hypomorphic allele, *hmp-1*(*fe4*), decreases actin binding *in vitro*. Using *hmp-1*(*fe4*) animals in a mutagenesis screen, we were then able to identify 11 intragenic suppressors of *hmp-1*(*fe4*) that revert actin binding to wild-type levels. Using homology modeling, we show that these amino acids are positioned at key conserved sites within predicted α-helices in the C terminus. Through the use of transgenic animals, we also demonstrate that HMP-1 residues 315–494, which correspond to a putative mechanotransduction domain that binds vinculin in vertebrate αE-catenin, are not required during epidermal morphogenesis but may aid efficient recruitment of HMP-1 to the junction. Our studies are the first to identify key conserved amino acids in the C terminus of α-catenin that modulate F-actin binding in living embryos of a simple metazoan.

The cadherin-catenin complex (CCC)[4] comprises a highly conserved set of proteins that mediates adhesion between contacting cells at adherens junctions. Proper development requires that cadherin-based adhesions be highly adaptable; they must be stable enough to transmit forces to the cell surface that drive cell shape changes and tissue architecture, but at the same time dynamic enough to allow the cell rearrangements and morphogenetic movements required to shape the embryo (1, 2). Maintenance of intercellular adhesions is also important in adult organisms, where loss of CCC proteins can result in tumorigenesis and metastasis (3, 4).

The CCC mediates intercellular adhesion through the calcium-dependent homophilic interactions of transmembrane cadherin receptors (5). Adhesive connections are stabilized through the association of the cadherin intracellular tail with p120-catenin, β-catenin, and α-catenin (6–10). α-Catenin localizes to the CCC through an N-terminal β-catenin binding site (11–15), whereas a C-terminal actin-binding domain (ABD) associates the CCC with the F-actin cytoskeleton (16–18). α-Catenin has three domains with significant homology to the protein vinculin, and are therefore termed vinculin homology (VH) domains (19). The ABD of α-catenin includes the VH3 domain. Although several studies have shown the absolute requirement of the α-catenin ABD in conferring full adhesive activity and cytoskeletal interaction to the CCC (16, 17, 20–23), it is unclear if F-actin attachment occurs mainly through direct binding to α-catenin or through other actin-binding proteins in an α-catenin-dependent fashion. Several other actin-binding proteins bind to vertebrate α-catenin, including vinculin (16,

* This work was supported, in whole or in part, by National Institutes of Health Grant RO1 GM58038 (to J. D. H.), American Heart Association Grant 0815662G (to S. L. M.), Wellcome Trust Grant 073317/Z/03/Z (to J. P.), and a Michael Guyer postdoctoral fellowship (to A. M. L.).
[S] This article contains supplemental "Experimental Procedures," Figs. S1–S4, and Tables S1 and S2.
[1] Present address: Dept. of Cell Biology, University of Virginia, Charlottesville, VA 22908.
[2] Present address: Dept. of Metabolism and Aging, The Scripps Research Institute, Jupiter, FL 33458.
[3] To whom correspondence should be addressed: Dept. of Zoology, University of Wisconsin, 1117 W. Johnson St., Madison, WI 53706. E-mail: jdhardin@wisc.edu.

[4] The abbreviations used are: CCC, cadherin-catenin complex; LOF, loss-of-function; CFB, circumferential actin filament bundle; VH, vinculin homology; ABD, actin-binding domain; FRAP, fluorescence recovery after photobleaching; EMS, ethane methyl sulfonate; PDB, Protein Data Bank.

24–28), α-actinin (15, 16, 29), ZO-1 (16, 30), afadin (18), formin-1 (31), and EPLIN (32). Binding sites on α-catenin have been partially mapped for several of these proteins; some lie outside of the C terminus, whereas others overlap with the ABD (15, 16, 18, 24–32). It is thus possible that interactions between α-catenin and the actin cytoskeleton occur through both direct and indirect mechanisms, and the contribution of each depends on the cellular context (33). Recently αE-catenin has been shown to be a coactivator of vinculin (26), and the binding of vinculin to αE-catenin has been found to be force-dependent, suggesting a role for αE-catenin in mechanotransduction (22). However, it is unclear whether or not this function is conserved among other α-catenins.

Detailed *in vivo* analysis of α-catenin function in mammals has been difficult due to its requirement in early development (23). *Cre*-mediated recombination has allowed several studies to temporally control conditional ablation of α-catenin in specific tissues (34, 35); however, this method has only been used to create null mutants rather than to examine requirements for specific domains or single amino acids of α-catenin.

Caenorhabditis elegans provides a unique opportunity to study the requirements for α-catenin function in a simple metazoan. This powerful invertebrate model system is amenable to mutagenesis and genetic manipulation, and its transparency allows the visualization of complex morphogenetic movements during development. There are conserved *C. elegans* homologs for each of the main CCC proteins: HMR-1/cadherin, JAC-1/p120-catenin, HMP-2/β-catenin, and HMP-1/α-catenin (36, 37). HMP-1 is 35–38% identical to vertebrate and invertebrate α-catenins (36). Moreover, unlike vertebrates, HMP-1 is the sole α-catenin homolog in *C. elegans,* removing any issues of functional redundancy. Mutations in *hmp-1* result in a characteristic defect during epidermal morphogenesis, when Rho-dependent actomyosin-mediated contractile forces are transmitted along circumferential actin filament bundles (CFBs) to cell-cell junctions to drive the cell shape changes necessary for elongation of the embryo. Strong zygotic loss-of-function (LOF) *hmp-1* mutants exhibit loss of junctional proximal actin and detachment of CFBs, which leads to the formation of dorsal folds in the epidermis (the Humpback phenotype). Removal of both maternal and zygotic HMP-1 via RNAi or through germline mosaics results in a more severe phenotype, in which ventral epidermal cells fail to properly adhere to one another. This results in anterior rupture of the embryo at the onset of elongation, mimicking mutations in *hmr-1*/E-cadherin (36).

Here we identify discrete regions and single amino acids in the HMP-1/α-catenin ABD that modulate attachment to F-actin. Through characterization of *hmp-1* alleles isolated in a previous EMS mutagenesis screen (36), we have identified residues 687–742, 826–927, and 802, all within the ABD, as critical to proper HMP-1 function and actin binding during epidermal morphogenesis. Utilizing a hypomorphic allele, *hmp-1(fe4)*, we have also used EMS mutagenesis to identify second site mutations in the ABD that alleviate the *fe4* weak LOF phenotype. Through *in vitro* actin cosedimentation assays, we find that these mutations are able to rescue the ability of HMP-1 to bind F-actin directly. Through the use of transgenic deletion constructs, we also show that residues 315–494 of HMP-1, the putative vinculin-binding domain, are not essential for embryonic development. Fluorescence recovery after photobleaching (FRAP) analysis of embryos expressing a construct lacking this region nevertheless suggests that this domain may be required for efficient targeting of HMP-1 to the CCC.

EXPERIMENTAL PROCEDURES

Strains and Alleles—C. elegans strains were cultured using standard protocols (38). The Bristol strain N2 was used as wild-type. The strong zygotic loss-of-function *hmp-1* mutants were derived from a previous EMS mutagenesis screen (36). For a complete list, see supplemental "Experimental Procedures."

To determine the ability of different domains of HMP-1 to rescue *hmp-1*(*zu278*), *hmp-1*::*gfp* deletion constructs were microinjected (39) at 1 ng/μl along with *rol-6*(*su1006*) (79 ng/μl) and noncoding DNA (F35D3, 20 ng/μl) into the gonads of either N2 or SU370 (+/*nT1[qIs5I]* IV; *hmp-1(zu278)/nT1[qIs5I]* V) hermaphrodites. Extrachromosomal arrays maintained in N2 were crossed into SU370 hermaphrodites later. If *hmp-1*(*zu278*) mutant embryos were rescued to viability, a separate line was maintained. For a complete list of strains, see supplemental "Experimental Procedures."

hmp-1(*fe4*) suppressors were isolated from nonclonal screens by mutagenizing *hmp-1*(*fe4*) homozygotes with 50 mM EMS and starting cultures with individual mutagenized adults. Once the F2 generation had reached adulthood, plates were screened by eye for morphologically wild-type animals. In some cases, the animals picked still segregated a proportion of Vab progeny, suggesting either that they were heterozygous and that the mutations might be dominant/semi-dominant, or that the suppressor effect was incompletely penetrated. In each case we were able to establish strains that segregated almost completely wild-type animals, indicating that the former explanation was more likely. Subsequent outcrosses with unmutagenized *hmp-1*(*fe4*) homozygotes confirmed this assessment.

Allele Sequencing—For strong LOF alleles, individual homozygous *hmp-1* mutant embryos were isolated based on phenotype and treated for 2 min with a 20 mg/ml of chitinase solution. If hatchoids were chosen, no chitinase was used. Embryos were transferred to 5 μl of single worm lysis buffer and frozen for 15 min at 80 °C, then lysed at 65 °C for 1 h followed by 95 °C for 15 min. Embryonic lysate was used to PCR amplify fragments of *hmp-1* and the products were cloned using the pCR8/GW/TOPO-TA cloning kit (Invitrogen, K250020). Clones were miniprepped and DNA was sequenced via Sanger sequencing through the University of Wisconsin-Madison Biotechnology Center.

For *fe4* intragenic suppressors, genomic DNA was amplified from single worm lysates derived from each suppressor mutant strain using primer pairs hmp1ex1/3S-3AS, hmp1ex4/5S-5AS, hmp1ex6–1/6–2, hmp1ex7–1/7–2 and hmp1ex8–1/8–2 (see supplemental "Experimental Procedures" for sequences), which amplify exons 1–3, 4–5, 6, 7, and 8, respectively. The resulting PCR products were sequenced directly. This also allowed the verification of the presence of the original *fe4* mutation. In only one strain was the *fe4* mutation found to be absent, suggesting that this was a revertant.

Staining—Embryos were isolated from plates and gravid hermaphrodites with 0.5% NaOCl in 250 mM NaOH for 5 min followed by three washes in distilled deionized water. For phalloidin staining, embryos were mounted on poly-L-lysine-coated ring slides and fixed with 4% paraformaldehyde, 0.1 mg/ml of lysolecithin, 48 mM PIPES, pH 6.8, 25 mM HEPES, pH 6.8, 2 mM $MgCl_2$, and 10 mM EGTA for 20 min and then washed three times with PBS. Embryos were incubated in the dark with 1:20 Alexa 555:phalloidin in PBST overnight at 4 °C, then washed three times with PBS before being covered with antifade reagent and sealed with nail polish.

For antibody staining, embryos were mounted on poly-L-lysine-coated ring slides and covered with a coverslip. Slides were quick frozen for 10 min on dry ice, then the coverslips were removed with a razor blade. Slides were immediately transferred to methanol at −20 °C for 5 min, acetone at −20 °C for 5 min, and PBST at room temperature for 5 min, followed by two additional PBST washes. Embryos were incubated with 1:3000 rabbit anti-HMP-1 and 1:20 mouse anti-AJM-1 (MH27) in 0.5% milk/PBST in the dark overnight at 4 °C. Slides were washed three times with PBST then incubated in the dark for 4 h at room temperature with 1:50 anti-rabbit Texas Red and 1:50 anti-mouse FITC in 0.5% milk/PBST. Slides were washed three times with PBST before being covered with antifade reagent and sealed with nail polish.

Mutant Constructs—Using an existing *hmp-1*::*gfp* containing the endogenous promoter,[5] targeted in-frame deletions were created using site-directed mutagenesis. Forward and reverse primers flanking the region to be deleted were used to create a linear PCR product. Subsequent phosphorylation and ligation created a circular plasmid that was transformed into DH5α competent cells. Deletion-positive clones were identified via gel electrophoresis and sequencing.

For the actin cosedimentation assays, a previously published *gst*::*hmp-1*(*677–927*) (21) construct was used to clone the *hmp-1*(*fe4*) mutation with Phusion polymerase via a circle PCR method. The second site intragenic suppressor mutations were cloned into the *hmp-1*(*fe4*) construct. The mutations were confirmed through sequencing after the mutant constructs were transformed into BL21(DE3) protein-expressing cells (Stratagene).

Imaging—Embryos were isolated from gravid hermaphrodites, mounted on a 5% agarose slide, and aged at 20–25 °C until the onset of morphogenesis. For four-dimensional differential interference contrast microscopy, embryos were imaged using 1-μm slice spacing at 3-min intervals using a Nikon Eclipse E600 microscope with a ×60/1.45 NA oil objective at 20 °C with a Macintosh computer running ImageJ using custom macros/plugins (available at worms.zoology.wisc.edu/research/4d/4d.html). For fluorescent imaging, a Perkin-Elmer UltraView spinning disk confocal microscope and software, using a Nikon Eclipse E600 microscope and Hamamatsu ORCA-ER camera, was used to collect images of GFP expressing embryos, using 0.8-μm slices at 3-min intervals with a ×60/1.45 NA oil objective at 20 °C. Phalloidin (0.2 μm slices) and antibody staining (0.6 μm slices) images were collected with the same confocal microscope using a ×100/1.45 NA oil objective.

Fluorescence Recovery After Photobleaching—Transgenic embryos were isolated from gravid hermaphrodites, mounted on 5% agarose slide, and aged at 20 °C for 4 h or until the onset of elongation. An Olympus Fluoview 1000 confocal microscope with SIM scanner was used to bleach and image GFP expressing embryos at <25 °C with a ×60 oil objective at zoom 3, with images taken every 1.1 s. At 1.25–1.5-fold elongation, the seam-seam junction of a seam cell was bleached and allowed to recover. Collected images were analyzed in ImageJ using the FRAP profiler plug-in (available at worms.zoology.wisc.edu/research/4d/4d.html). Normalized data were further analyzed in F_{calc}[6] and Microsoft Excel. A Student's *t* test was used to determine statistical significance.

Protein Expression and Purification—pGEX-TEV *gst* plasmids were transformed into BL21(DE3) bacterial cells and induced for protein expression by 0.1 mM isopropyl 1-thio-β-D-galactopyranoside at 30 °C. Cells were lysed by sonication in lysis buffer (50 mM Tris, pH 8.0, 300 mM NaCl, 5 mM DTT, 2 mM EDTA, 2 mM Benz-HCl, and 1 mM PMSF) and soluble fractions were incubated with glutathione-agarose beads. Beads were washed with PBSTR (1× PBS, 0.05% Tween 20, 5 mM DTT) and proteins were eluted from the beads with elution buffer (20 mM Tris, pH 8.5, 150 mM NaCl, 2 mM EDTA, 1 mM DTT, 10% glycerol, 0.3% glutathione). Concentrations were measured using a standard Bradford assay.

Actin Assays—G-actin from rabbit skeletal muscle (Cytoskeleton, Inc., AKL99) was polymerized into F-actin for 1 h at RT in actin polymerization buffer (5 mM Tris, pH 8.0, 0.2 mM $CaCl_2$, 0.5 mM DTT, 50 mM KCl, 2 mM $MgCl_2$, 1.2 mM ATP). 5 μM proteins of interest were incubated with 2 or 10 μM F-actin in reaction buffer (20 mM Tris, pH 8.5, 150 mM NaCl, 2 mM EDTA, 1 mM DTT, 10% glycerol, 0.2 mM ATP, 0.2 mM $CaCl_2$) for 30 min at RT. Reactions were pelleted at 100,000 × *g* for 20 min. Supernatant and pellet samples were prepared with the same dilution in Laemmli sample buffer and run on an 8% SDS-PAGE gel, then stained with Coomassie Blue. Band intensities were measured and quantified using ImageJ, then analyzed in Microsoft Excel. A Student's *t* test was used to determine statistical significance.

Homology Modeling—HMP-1 amino acids 677–927 were used to perform a BLAST search against the Protein Data Bank (PDB) to identify a suitable template structure for homology modeling. The tail of metavinculin had the highest homology (PDB code 3MYI, Chain A). This structure was used as a template to model HMP-1 amino acids 699–864 with SWISS-MODEL. The resulting PDB file was then viewed and analyzed using MacPyMOL (66).

RESULTS

Sequencing of Strong LOF hmp-1 Alleles Identifies Lesions That Perturb the C-terminal ABD—To begin dissecting HMP-1/α-catenin function *in vivo*, we obtained 8 largely uncharacterized *hmp-1* alleles from a previous EMS mutagenesis screen (36). These alleles include *zu242*, *zu244*, *zu349*, *zu402*, *zu365*,

[5] J. Simske, unpublished data.

[6] R. Sara, personal communication.

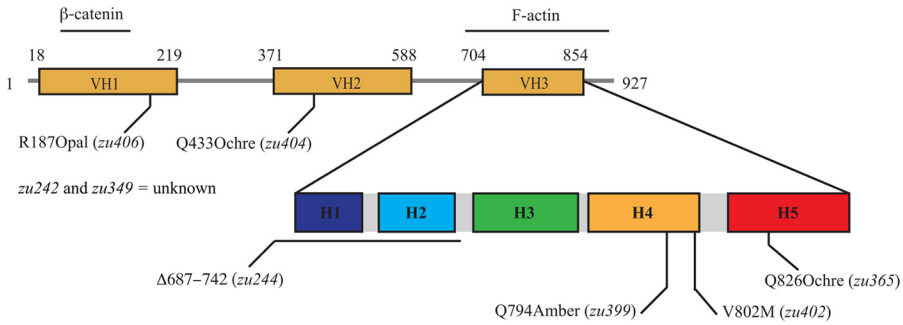

FIGURE 1. **Sequencing of strong LOF *hmp-1* alleles identifies lesions that perturb the C-terminal ABD.** Schematic representation of the location of each mutation within HMP-1. The positions of the five α helices (predicted on the basis of homology modeling with the homologous region of vinculin, see Fig. 6) within the ABD are indicated (H1–5). Although two lesions lie upstream of the ABD (*zu406* and *zu404*), both of these are premature stop codons that would presumably delete the C terminus without affecting the localization signal (β-catenin binding site). The lesions in all other alleles lie within the ABD and include not only nonsense mutations (*zu399* and *zu365*), but also a small deletion (*zu244*) and a missense mutation (*zu402*).

zu399, *zu404*, and *zu406*. Using four-dimensional differential interference contrast confocal microscopy, every allele was found to exhibit a strong zygotic LOF Humpback phenotype as previously described (36) (supplemental Fig. S1). On rare occasions, ruptures from the ventral surface were observed for *hmp-1*(*zu242*), *hmp-1*(*zu365*), and *hmp-1*(*zu399*) (data not shown). In these cases, there appeared to be a failure of ventral cells to properly adhere at the ventral midline. Late posterior ruptures were also occasionally observed for *hmp-1*(*zu365*) and *hmp-1*(*zu399*), in which cells begin to leak out of the posterior end of the embryo after the embryo has formed dorsal humps (data not shown).

Each of the alleles originally identified by Costa *et al.* (36) is recessive and zygotic lethal; however, we noticed that for certain alleles, a portion of homozygous mutant progeny were no longer contained in an eggshell (supplemental Fig. S2*A*) and in some cases exhibited muscle activity (data not shown). As embryos mature in the eggshell, they begin to secrete enzymes that aid in hatching (40). Although such embryos therefore appear to have lived long enough to degrade the eggshell, careful observation over time confirmed these hatched embryos ("hatchoids") eventually die. The percentage of *hmp-1* homozygous mutants that become hatchoids varies among alleles (supplemental Fig. S2*B*) and indicates that there are subtle differences in the overall time of death.

Next we sequenced the *hmp-1* locus in homozygous *hmp-1* mutants to determine the genetic lesion associated with each allele (Fig. 1 and supplemental Table 1). Despite analyzing the genomic region 5 kbp upstream and 0.3 kbp downstream of *hmp-1*, we were unable to identify the molecular lesions that correspond to *hmp-1*(*zu242*), the only allele for which no protein expression was detectable (see Fig. 2), or *hmp-1*(*zu349*). We presume that *hmp-1*(*zu242*) and *hmp-1*(*zu349*) involve mutations in enhancer elements that lie far from the *hmp-1* locus itself.

Several new truncation mutants were identified through sequencing. *hmp-1*(*zu404*) and *hmp-1*(*zu406*) both have nonsense mutations in the N-terminal half of *hmp-1* and are predicted to express truncated proteins at amino acids 433 and 187, respectively (Fig. 1). A nonsense mutation was also identified in *hmp-1*(*zu399*), which is predicted to create a truncated protein in the ABD at amino acid 794 (Fig. 1). This mutation is one residue before the truncation previously reported for *hmp-1*(*zu278*) (21). The most C-terminal mutation we identified was *hmp-1*(*zu365*) (Fig. 1), and is predicted to encode another premature stop codon at residue 826. It is clear from these truncation mutants that the ABD of HMP-1 is critical for proper epidermal morphogenesis, especially the C-terminal tail, from amino acids 827 to 927.

Only one missense mutation was identified among the alleles, *hmp-1*(*zu402*) (Fig. 1). This mutation is also in the ABD (Fig. 1) and is upstream of another known missense mutation, *hmp-1*(*fe4*) (37). Because the S823F mutation in *hmp-1*(*fe4*) was found to be in a conserved SLIQ motif (37), we used a multiple sequence alignment to determine whether the V802M mutation in *hmp-1*(*zu402*) also lies in a conserved motif. Indeed, this mutation occurs at a valine residue in an SKVKA motif that is absolutely conserved in α-catenins from five diverse species, including humans, and is also conserved in human vinculin (supplemental Fig. S3). Another intriguing lesion was found in *hmp-1*(*zu244*); a 56-amino acid in-frame deletion at the extreme N terminus of the ABD, Δ687–742 (Fig. 1). This 56-amino acid deletion leaves the C-terminal tail intact, yet homozygotes display 100% embryonic lethality. This is the first evidence that the N-terminal portion of the ABD is critical to α-catenin function. In summary, HMP-1 residues 687–742 and 802, as well as the C-terminal tail, residues 827–927, are important for proper epidermal morphogenesis.

Strong LOF hmp-1 Alleles Express Mutant Protein—Our sequence analysis suggests that the HMP-1 ABD is essential for function, as various mutations or deletions in the C terminus affect epidermal morphogenesis. It is possible that nonsense-mediated decay mechanisms prevent some of these deleterious mutant proteins from being expressed, or that the protein products are mislocalized, so we next examined protein expression and localization in the mutant alleles. Using anti-AJM-1 antibody as a marker for cell-cell contacts (Fig. 2, *A–E* and *K–N*), double antibody staining of *hmp-1* homozygous mutants with anti-HMP-1 polyclonal antibodies revealed variations in HMP-1 protein expression and localization among alleles (Fig. 2, *F–J* and *O–R*). In a WT embryo (Fig. 2, *A* and *F*), both AJM-1 (Fig. 2*A*) and HMP-1 (Fig. 2*F*) localize to seam-dorsal, seam-seam, and seam-ventral contacts, although AJM-1 is basal to HMP-1 (41, 42). In *hmp-1*(*zu242*) (Fig. 2, *B* and *G*), punctate

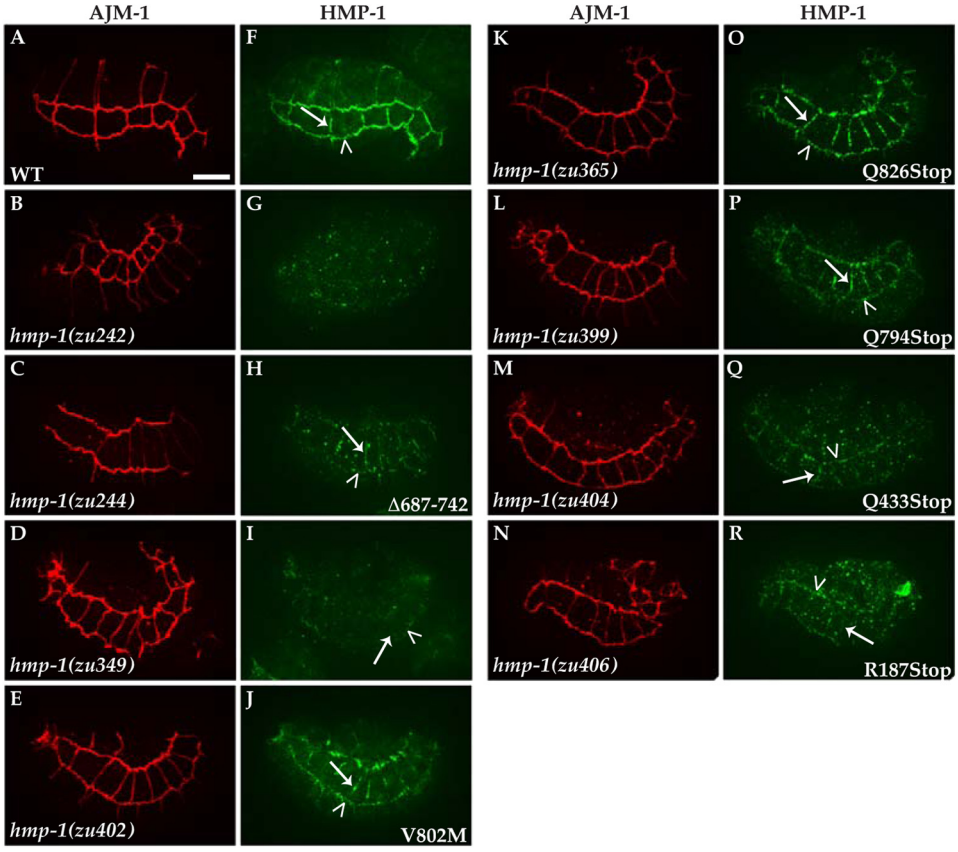

FIGURE 2. **Protein expression in strong LOF hmp-1 mutants.** *A–R*, double antibody staining of representative homozygous mutant embryos for each allele. Anterior is *left*, dorsal is *up*. Anti-AJM-1 in *red* (*A–E* and *K–N*); anti-HMP-1 in *green* (*F–J* and *O–R*). Anti-AJM-1 staining marks cell-cell contacts. *Scale bar* is 10 μm. *Arrows* indicate seam-seam junctions and *carets* indicate seam-ventral or seam-dorsal junctions. Note the puncate expression in *G* and the lack of any discernible HMP-1 localization along cell-cell contact sites. Background puncta can also be seen in *H* and *P-R*, but unlike *G*, there is also HMP-1 localized to junctions. There is very little junctional localization in *I*, but this varies among embryos for this allele. Although *J* has diffuse background signal, both *J* and *O* exhibit fairly strong HMP-1 staining at junctions.

HMP-1 expression can be observed (Fig. 2*G*), but no discernible localization along cell-cell contacts when compared with AJM-1 (Fig. 2*B*). *hmp-1*(*zu244*), *hmp-1*(*zu399*), *hmp-1*(*zu404*), and *hmp-1*(*zu406*) also exhibit this same punctate HMP-1 distribution, but also exhibit junctional HMP-1 (Fig. 2, *H* and *P–R*). Embryos homozygous for the other allele for which we could not identify a lesion in the coding region, *hmp-1*(*zu349*) (Fig. 2, *D* and *I*), display a variable, faint pattern of HMP-1 along cell-cell contacts (Fig. 2*I*). In summary, every allele but one (*hmp-1*(*zu242*), Fig. 2, *B* and *G*) has at least some localization of HMP-1 along cell contacts. Amino acids 1–186 appear to be sufficient for localization (*hmp-1*(*zu406*); Fig. 2*R*), which matches our previously published structure-function results that amino acids 13–185 are required for localization (21). However, even though these mutant HMP-1 proteins can localize, perturbations of the C terminus appear to abrogate proper HMP-1 function.

F-actin Defects Are Most Severe in Homozygous hmp-1(zu242) and hmp-1(zu406) Mutants—Previous work has shown that elongation defects in *hmp-1* homozygous mutants can be attributed to disorganization of the actin cytoskeleton (21, 36, 37), but these studies used mutants (*hmp-1*(*fe4*), *hmp-1*(*zu278*)) that produce either missense or late C terminally truncated proteins (21, 37). To determine whether other mutants display stronger F-actin defects, we stained homozygous *hmp-1* mutants with fluorophore-conjugated phalloidin (Fig. 3). In WT embryos (Fig. 3*A*), parallel, equally spaced CFBs insert into a network of junctional proximal actin concentrated along the seam-dorsal and seam-ventral boundaries (*red arrow*). In mutants examined, there is a lack of junctional proximal actin, leaving gaps at the seam-dorsal and seam-ventral boundaries (*red arrows*; Fig. 3, *B–I*). The CFBs are also not as evenly spaced, and often appear thicker, with large intervening gaps (*blue arrowheads*, Fig. 3, *B–I*). Although these general characteristics match previous data from *hmp-1*(*zu278*) (21, 36), both *hmp-1*(*zu242*) and *hmp-1*(*zu406*) homozygotes display even more severe F-actin phenotypes. In *hmp-1*(*zu242*) homozygotes there are areas that exhibit detachment of CFBs from the junction (*left red arrow*, Fig. 3*B*), but other areas show much larger regions devoid of F-actin (*right red arrow*, Fig. 3*B*). The same can be seen for *hmp-1*(*zu406*) (*red arrow*, Fig. 3*I*). *hmp-1*(*zu242*) also exhibits much thicker CFBs or what appear to be laterally collapsed densities of F-actin (Fig. 3*B*). In summary, mutants exhibiting a complete lack of HMP-1 at junctions (*hmp-1*(*zu242*)) and those expressing a protein that is predicted to truncate the 740 C-terminal amino acids of HMP-1 (*hmp-1*(*zu406*)) have more severe F-actin defects compared with other *hmp-1* alleles.

Intragenic Suppressors of hmp-1(fe4) All Map to the ABD—Homozygotes of a hypomorphic allele, *hmp-1*(*fe4*), exhibit only

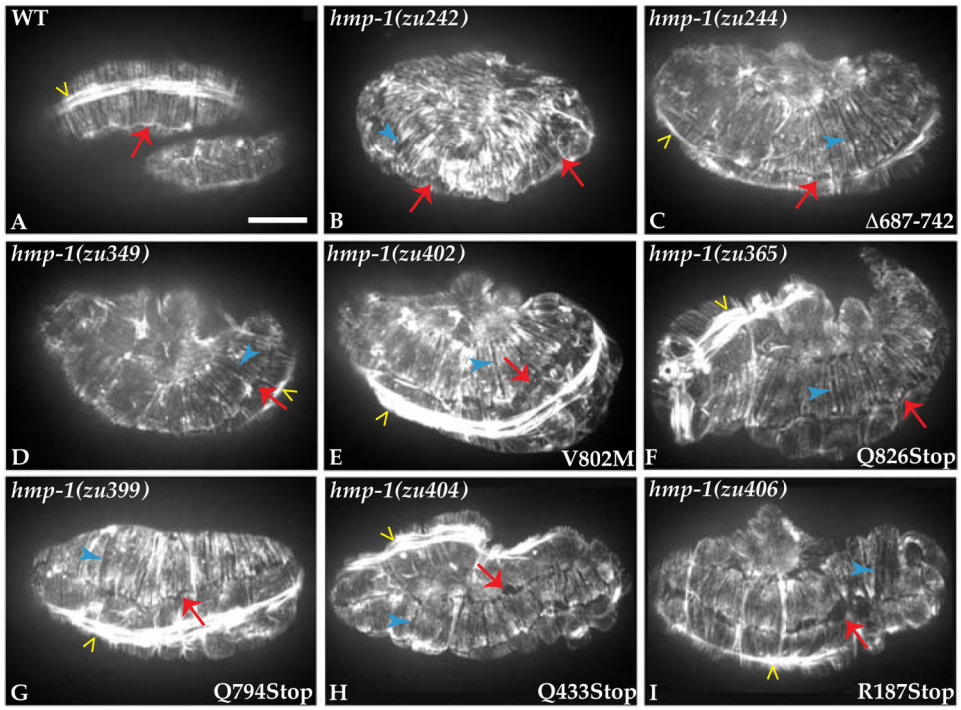

FIGURE 3. **F-actin defects are most severe in *hmp-1*(*zu242*) and *hmp-1*(*zu406*) mutant embryos.** *A–I*, staining with fluorophore-conjugated phalloidin to visualize F-actin organization in homozygous *hmp-1* embryos. Anterior is *left*, dorsal is *up*. *Scale bar* = 10 μm. *Yellow carets* indicate the underlying muscle; *red arrows* point to junctional proximal actin near adherens junctions or a lack thereof; *blue arrowheads* mark gaps between CFBs. In the wild-type embryo (*A*), parallel CFBs are visible as well as junctional proximal actin, which has concentrated along the seam-dorsal boundary (*red arrow*). *B–I*, in all of the *hmp-1* mutants there is a lack of junctional proximal actin, leaving gaps at the seam-dorsal and seam-ventral boundaries (*red arrows*). These gaps are especially pronounced in *B* (*right red arrow*) and *I*. The mutants also display large gaps between CFBs (*blue arrowheads*) as well as thicker bundles. Thicker bundles or large accumulations of F-actin appear more pronounced in *B*.

~70% embryonic lethality compared with 100% observed with strong LOF mutants. This feature has made *hmp-1*(*fe4*) a valuable tool in identifying genetic interactors through suppressor and enhancer screens (37, 43–46). Using EMS mutagenesis, we identified several dominant intragenic suppressors of *hmp-1*(*fe4*) (Fig. 4 and supplemental Table S2). Suppressor mutations were outcrossed using a strain homozygous for both *hmp-1*(*fe4*) and an integrated GFP transgene (*mls10*), both on chromosome V. Although some suppressors are clearly extragenic, extragenic suppressors partially characterized thus far appear to have no phenotypes and have not been analyzed further.[7] Many suppressors, however, mapped to the same genetic region as *hmp-1*. Outcrossing and subsequent sequencing confirmed these lesions are not revertants of *hmp-1*(*fe4*) and that they are located in the C-terminal coding region of *hmp-1* (Fig. 4). Although most of the intragenic suppressors are missense mutations, a few alleles are nonsense mutations C-terminal to the VH3 domain (Fig. 4). Multiple sequence alignment reveals a cluster of suppressors in a conserved FTRG motif, but the rest appear to be scattered among other conserved residues in the ABD (supplemental Fig. S3).

Lesions in hmp-1(fe4) and the Intragenic Suppressors Identify Specific Residues That Modulate HMP-1 F-actin Binding—*hmp-1*(*fe4*) encodes a missense mutation, S823F, which does not affect accumulation of junctional proximal actin in mutant embryos but does cause thicker and sparser CFBs (37). The equivalent mutation in vertebrates, S817F, was reported to increase the avidity of the α-catenin ABD for F-actin by 37% in a high speed pelleting assay (47). This is surprising given the strong evidence that *hmp-1*(*fe4*) is a weak LOF mutant (37, 43–46). If HMP-1 protein from *hmp-1*(*fe4*) homozygous mutants indeed has a higher binding affinity for F-actin than WT, and this is the cause of the thicker CFBs, then the intragenic suppressor mutations would be predicted to decrease the binding affinity to near WT levels. Conversely, if the *hmp-1*(*fe4*) mutation decreases F-actin binding affinity, the suppressors would be predicted to increase binding affinity. To determine how these secondary mutations restore proper HMP-1 function, we purified bacterially expressed protein consisting of HMP-1 amino acids 677–927 fused to GST, or the same fragment carrying the *hmp-1*(*fe4*) S823F mutation alone, as well as in tandem with the second site mutations identified in two of the intragenic suppressor mutants (N853K, found in *hmp-1*(*fe29*); F735C, found in *hmp-1*(*fe27*)). We showed previously that a recombinant protein containing HMP-1 residues 677–927 binds avidly to F-actin in a high speed actin cosedimentation assay (21), so we employed the same technique here to determine the avidity of these mutant constructs for F-actin (Fig. 5, *A* and *B*). We found a statistically significant decrease in the percentage of HMP-1 ABD bound to F-actin (pellet fraction = P; Fig. 5*A*) when the S823F mutation found in *hmp-1*(*fe4*) is present compared with WT (Fig. 5*B*). This is most prominent at 2 μM F-actin, where binding is decreased an average of 34.1%, but even under saturating conditions (10 μM F-actin), binding is still decreased an average of 7.3%. When the *hmp-1*(*fe4*) S823F mutation is in tandem with either the *hmp-*

[7] C. Lockwood and J. Hardin, unpublished data.

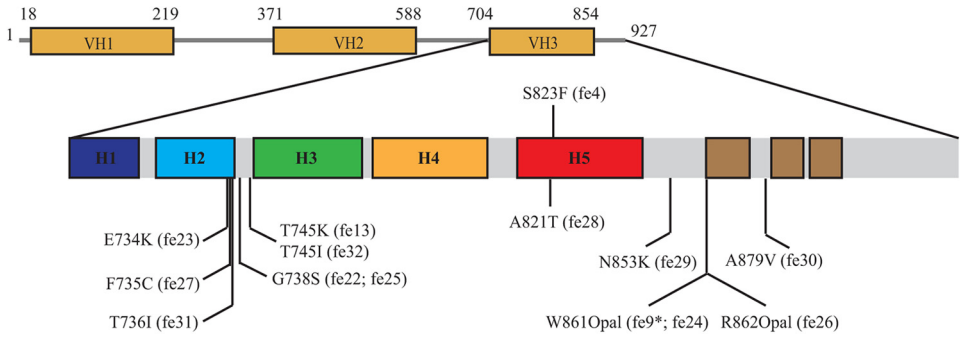

FIGURE 4. **Intragenic suppressors of *hmp-1*(*fe4*) all map to the ABD.** Schematic representation of the C-terminal ABD of HMP-1 showing the location of *fe4* and the suppressor mutations. The positions of the five α helices (predicted on the basis of homology modeling with the homologous region of vinculin, see Fig. 6) are indicated (*H1–5*). The three conserved motifs specific to the α-catenin tail are shaded *brown*. *, the *fe9* mutation was recovered linked with another mutation, fe14, a missense mutation, $Glu^{616} \rightarrow Lys$, which is located outside of the VH3 domain.

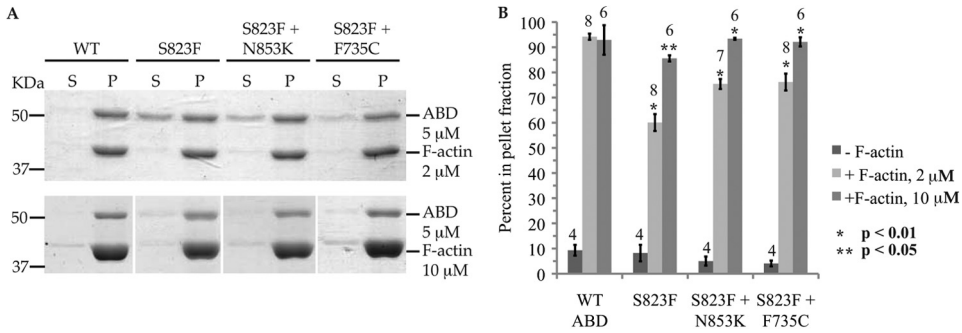

FIGURE 5. **Lesions in *hmp-1*(*fe4*) and the intragenic suppressors identify specific residues that modulate HMP-1 F-actin binding.** *A,* Coomassie-stained SDS-PAGE of actin cosedimentation experiments. *S* = supernatant fraction, *P* = pellet fraction. In this assay, protein bound to F-actin appears in the pellet fraction, whereas unbound protein remains in the supernatant. *B*, quantitation of data from *A*. The percentage of ABD protein found in the pellet fraction is compared at two concentrations of F-actin. *Error bars* indicate S.D, *numbers* indicate *n* values for each column. Note that at both F-actin concentrations, the binding of GST::HMP-1ABD is decreased significantly when the *hmp-1*(*fe4*) S823F mutation is present compared with WT. At 2 μM F-actin, this decrease is partially reverted with the addition of the second site intragenic suppressor mutations, and completely reverted to WT levels at 10 μM F-actin. Significance was determined by Student's *t* test: *, $p < 0.01$; **, $p < 0.05$.

1(*fe29*) N853K mutation or the *hmp-1*(*fe27*) F735C mutation, there is also a statistically significant increase in the amount of HMP-1 ABD bound to F-actin (*P*, Fig. 5*A*) when compared with *hmp-1*(*fe4*) S823F alone (Fig. 5*B*). At 2 μM F-actin, the *hmp-1*(*fe29*) N853K and *hmp-1*(*fe27*) F735C mutations increase actin binding an average of 15.3 and 16.1%, respectively. Although at this concentration the intragenic suppressor mutations do not restore actin binding to fully wild-type levels, at 10 μM F-actin the double mutants are indistinguishable from wild-type. In summary, *hmp-1*(*fe4*) S823F decreases the ability of HMP-1 to bind F-actin, and the intragenic suppressor mutations revert this binding to nearly wild-type levels. Based on these results, we conclude that the *fe4* intragenic suppressors identify amino acids that are capable of modulating the ability of HMP-1 to bind F-actin.

Homology Modeling Identifies Conserved C-terminal Amino Acids Required for HMP-1 to Bind Actin—Locating the residues in the C terminus of HMP-1 that we identified genetically within the context of a three-dimensionally folded protein would provide significant further insight into how these residues function *in vivo*. No crystal structure exists for the ABD of α-catenin or HMP-1; however, homology of the C terminus relative to the solved structure of the vinculin tail domain has proven useful in the past (47), so we pursued this approach with HMP-1 using SWISS-MODEL (48). We used the protein sequence of the HMP-1 ABD domain to search the Protein Data Bank for a suitable template for homology modeling of the C terminus. Not surprisingly, our search recognized the tail of metavinculin, a muscle-specific isoform of vinculin, as the highest homology sequence. The tails of both vinculin and metavinculin form a five-helix antiparallel bundle (49, 50). Our homology model of the HMP-1 VH3 domain also identifies five α-helices (Fig. 6). In Fig. 6, these helices are numbered 1–5 from the N to C terminus and colored as blue (*1*), cyan (*2*), green (*3*), orange (*4*), and red (*5*).

We then mapped the C-terminal amino acids mutated in the strong LOF *hmp-1* alleles onto our homology model (Fig. 6, *A* and *B*). Residue 742 (*gray,* Fig. 6*A*) marks the last C-terminal amino acid deleted in *hmp-1*(*zu244*). Both helices 1 and 2 (Fig. 6*A*) would be deleted in these allele, whereas leaving the rest of the ABD intact. Interestingly, the missense mutation identified at residue 802 in *hmp-1*(*zu402*) lies adjacent to residue 823, the site of the missense mutation in *hmp-1*(*fe4*) (37) (*cyan* and *purple*, respectively; Fig. 6*B*). This implicates these specific residues in proper actin binding and HMP-1 function. The premature stop codon found at amino acid 794 in *hmp-1*(*zu399*) would completely remove this region, as well as the rest of the C terminus (*magenta*, Fig. 6*B*). Another nonsense mutation, identified at residue 826 in *hmp-1*(*zu365*), lies directly C-terminal to the *hmp-1*(*fe4*) site and may also perturb this region directly (*yellow*, Fig. 6*B*). Moreover, the model suggests a possible explanation for why the *hmp-1*(*zu244*) mutation affects actin bind-

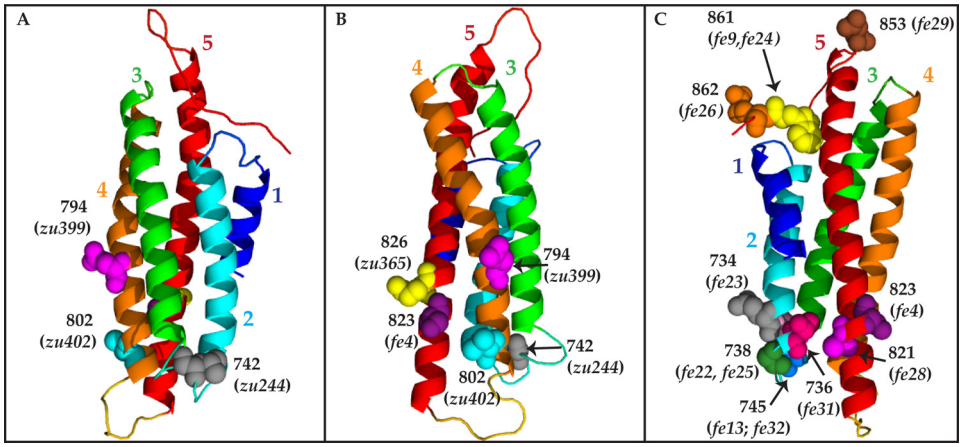

FIGURE 6. **Homology modeling of the HMP-1 VH3 domain provides insights into the possible function of certain regions and residues in the C terminus.** *A–C*, using the metavinculin VH3 domain crystal structure as a template (PDB code 3MYI, Chain A), the HMP-1 VH3 domain was modeled using SWISS-MODEL (48). Images were created using MacPyMOL (66). The tertiary structure of the VH3 domain contains a series of α-helices. The helices are numbered *1–5* from the N to C terminus and colored as *blue* (*1*), *cyan* (*2*), *green* (3), *orange* (*4*), and *red* (*5*), respectively. The residues mutated in *hmp-1* alleles are shown as space-filled molecules labeled with the amino acid number. *A*, residues mutated in identified strong LOF *hmp-1* alleles. Amino acid 742 marks the C-terminal end of the deletion found in *hmp-1*(*zu244*). The N-terminal limit of this deletion is beyond the VH3 domain, thus both helices 1 and 2 would be missing in this allele. *B*, a second view rotated around the vertical axis of the structure to more clearly show the locations of residues mutated in other strong LOF alleles. Note here that the missense mutation at residue 802 identified in *hmp-1*(*zu402*) is adjacent to another well characterized missense mutation at residue 823, *hmp-1*(*fe4*). *C*, residues mutated in *hmp-1*(*fe4*) and the intragenic suppressor alleles. Residue 879 (*fe30*) is not shown because it lies C-terminal to the sequence we were able to model. Note the cluster of suppressor mutation sites between helices 2 and 3, which lie behind the *hmp-1*(*fe4*) mutation site at residue 823. In addition, several suppressor sites are located on a C-terminal arm after helix 5 that lies above helix 1/2. Each of these clusters may indicate that the orientation of helix 5 is important for proper F-actin binding.

ing: if this face of the C terminus (helices 4 and 5; Fig. 6*B*) acts as a discrete binding site for F-actin, deletion of the N-terminal helices 1 and 2, as occurs in *hmp-1*(*zu244*) (Fig. 6*A*), may abrogate actin binding by changing the spatial orientation of the C-terminal helix 5 (Fig. 6*B*). It is also possible that N-terminal helices 1 and 2 are part of a continuous binding site distributed among the C-terminal helices 4 and 5 (Fig. 6*B*), and its removal abrogates strong F-actin binding.

We also used our homology model to investigate why second site, intragenic missense and nonsense mutations alleviate the phenotypic defects of *hmp-1*(*fe4*) mutants (Fig. 6*C*). Although the *hmp-1*(*fe4*) mutation at residue 823 (*purple*), and one suppressor mutation at 821 (*magenta*), lie on helix 5, a cluster of intragenic suppressor sites are located directly adjacent, at the end of helix 2 (Fig. 6*C*). As suggested for the LOF *hmp-1* alleles (Fig. 6, *A* and *B*), mutations in the N-terminal helix 2 may alter the position of the C-terminal helix 5 sufficiently to restore stable actin binding. Alternatively, N-terminal helix 2 may also be directly involved in binding to actin, and these mutations may increase the avidity of HMP-1 for F-actin enough to compensate for the original defect.

The two amino acids identified as nonsense mutations in *hmp-1*(*fe9*), *hmp-1*(*fe24*), and *hmp-1*(*fe26*), Trp-861 and Arg-862, are both located in the C-terminal arm past helix 5 that lies above N-terminal helices 1 and 2 (Fig. 6*C*). In vinculin, this C-terminal arm binds to acidic phospholipids and causes a conformational change in the tail that potentially relieves inhibition by the head domain, which may activate its ability to bind other proteins, such as talin (49). Removal of this C-terminal arm when only the vinculin tail is present does not affect actin binding (49), indicating that the conformational change in the tail apart from its context in the whole protein is not sufficient to affect actin binding. If the *hmp-1*(*fe4*) S823F mutation perturbs F-actin binding due to increased steric hindrance or blockage of other needed residues, then truncation of the C-terminal arm may result in a constitutively active HMP-1 with a more flexible ABD that allows a reorientation of residue 823. Binding of the C-terminal arm of HMP-1, which lies outside the VH3 domain, by a currently unknown ligand might also result in release of the intramolecular inhibition we previously reported for full-length, wild-type HMP-1 *in vitro* (21). It should be noted that an ABD construct lacking this same C-terminal arm region of αE-catenin(678–864) was not able to bind F-actin *in vitro* (18), which may indicate HMP-1 has retained functional similarity to vinculin in this capacity compared with αE-catenin.

The Putative Vinculin-binding Domain of HMP-1 Is Not Required for Epidermal Morphogenesis But Does Affect HMP-1 Mobility—The results we have reported thus far and those reported previously (21) clearly show that the HMP-1 ABD is critical for proper *C. elegans* development, but the function of more N-terminal domains is not well understood. We have previously shown that expression of a *hmp-1*::*gfp* construct driven by the endogenous *hmp-1* promoter can rescue a strong LOF mutant, *hmp-1*(*zu278*), which contains a Q795Stop mutation. However, deletion of the putative β-catenin binding site in this construct (HMP-1(Δ13–185)::GFP) results in its mislocalization to the cytoplasm, and as a result, it is not able to rescue homozygous *hmp-1*(*zu278*) mutants (21). To determine the importance of other regions, the same full-length *hmp-1*::*gfp* was used to create targeted in-frame deletions of other internal domains of HMP-1. These deletion constructs were expressed in the same strong LOF background, *hmp-1*(*zu278*), and homozygous mutants were identified by the absence of a pharyngeal GFP balancer. Transgenic mutant embryos were then analyzed using four-dimensional spinning disc confocal microscopy (Fig. 7).

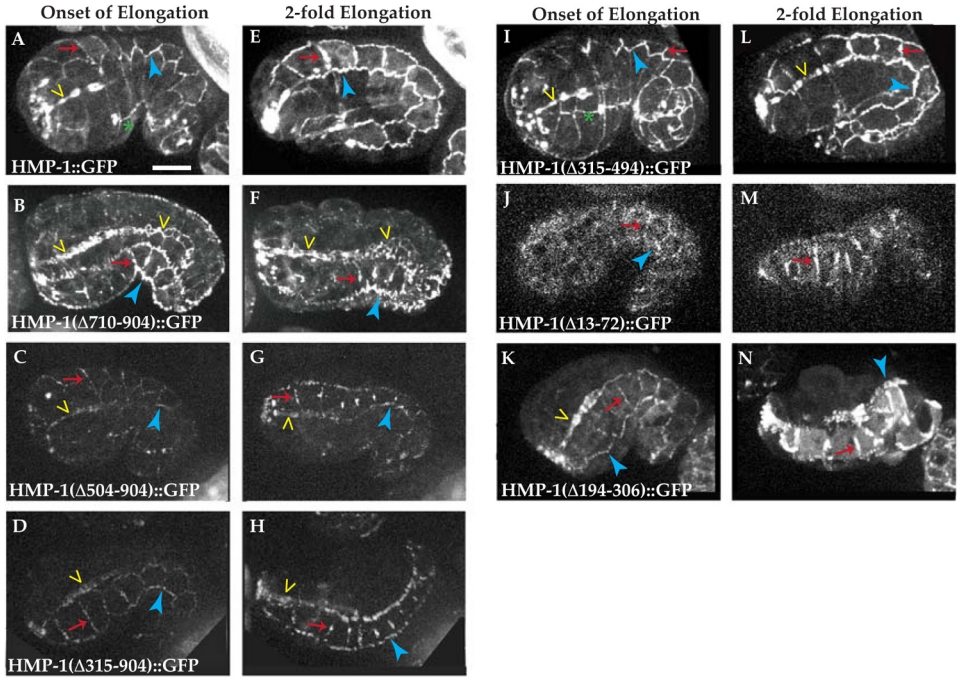

FIGURE 7. **HMP-1 residues 315–494 are not required for proper epidermal morphogenesis.** *A-N*, fluorescent spinning disk confocal microscopy of HMP-1::GFP deletion constructs expressed in homozygous mutant embryos carrying a strong loss-of-function allele, *hmp-1*(*zu278*). Anterior is *left*, dorsal is *up*. *Scale bar* = 10 μm. *Yellow carets* indicate the pharynx; *red arrows* point to seam-seam junctions; *blue arrowheads* point to seam-ventral junctions; *green stars* mark the ventral midline. *A–D* and *I–K*, transgene-expressing embryos at the onset of elongation. Note that like full-length HMP-1::GFP, all of the deletion constructs localize along cell-cell junctions. *E–H* and *L–N*, transgenic embryos at a time when wild-type embryos would be elongated 2-fold their original length. In *hmp-1*(*zu278*) homozygous mutants, embryos only reach 1.5-fold elongation before retracting dorsally and forming dorsal humps. Only the full-length HMP-1::GFP (*E*) and HMP-1(Δ315–494)::GFP (*L*) are able to rescue the *hmp-1*(*zu278*) phenotype and create viable adults.

At the onset of elongation, all of the transgenes localize to seam-seam, seam-ventral, and seam-dorsal junctions (Fig. 7, *A–D* and *I–K*), unlike HMP-1(Δ13–185)::GFP, which does not (21). We next assessed the ability of the constructs to rescue beyond the 1.5-fold stage of elongation. For comparison, a mutant embryo expressing the full-length HMP-1::GFP elongates 2-fold and maintains continuous transgene localization along cell-cell contacts (21) (Fig. 7*E*). Not surprisingly, constructs without the ABD are not able to rescue *hmp-1*(*zu278*) mutants, and localization becomes discontinuous as junctions become destabilized (Fig. 7, *F–H*). Two N-terminal regions not predicted to be involved in binding to β-catenin were also deleted, residues 13–72 and 194–306. Constructs lacking either of these regions properly localize to junctions (Fig. 7, *J, K, M,* and *N*), but surprisingly, are not able to rescue the mutant phenotype, even though they contain a functional ABD (Fig. 7, *M* and *N*). Because HMP-1(Δ13–185)::GFP does not localize to junctions (21), but HMP-1(Δ13–72)::GFP does, we conclude that residues 73–185 are required for proper localization of HMP-1.

The vinculin-binding domain of αE-catenin has been the subject of intense interest, because evidence suggests it is only exposed in response to tension (22). Interestingly, deletion of the corresponding domain of HMP-1, residues 315–494, did not effect the ability to rescue homozygous *hmp-1* mutants; localization of the transgene remains continuous as the mutant embryo elongates to 2-fold (Fig. 7*L*), similar to full-length HMP-1::GFP (Fig. 7*E*). The rescue by HMP-1(Δ315–494)::GFP is complete, and the transgenic homozygous mutants survive to adulthood and have viable progeny. Like HMP-1::GFP (21), HMP-1(Δ315–494)::GFP rescued adults exhibit an uncoordinated phenotype, but are otherwise developmentally normal with no body morphology defects (data not shown). We conclude that residues 315–494 are not essential for HMP-1 function during epidermal morphogenesis.

Although HMP-1(Δ315–494)::GFP rescues homozygous *hmp-1*(*zu278*) mutants as well as full-length HMP-1::GFP, we wondered if removing this domain nevertheless has sublethal effects on HMP-1 dynamics at junctions. We therefore performed FRAP analysis and compared the dynamics of recovery of HMP-1(Δ315–494)::GFP ($n = 8$) to full-length HMP-1::GFP ($n = 6$). For each experiment, a small region of interest in a lateral seam-seam junction was photobleached in a transgenic embryo elongated 1.25–1.5-fold (Fig. 8*A*). Full-length *HMP-1*::*GFP* shows fairly rapid recovery kinetics ($t_{½} = 9.1$ s) with a 69.3% mobile fraction (Fig. 8*B*). Although the population of mobile protein remains essentially the same in *HMP-1*(*Δ315–494*)::*GFP* (mobile fraction = 72.0%), fluorescence recovery was much slower ($t_{½} = 51.2$ s) (Fig. 8*B*). This is clearly seen in a co-plot of the point means for each transgene (supplemental Fig. S4). In conclusion, whereas *HMP-1*(*Δ315–494*)::*GFP* is sufficiently functional to rescue the developmental defects seen in *hmp-1*(*zu278*) mutant embryos, its mobility is impaired compared with full-length HMP-1::GFP.

DISCUSSION

We have previously shown that HMP-1/α-catenin has conserved functions in adhesion-dependent processes during *C. elegans* embryogenesis: the N terminus is required for localiza-

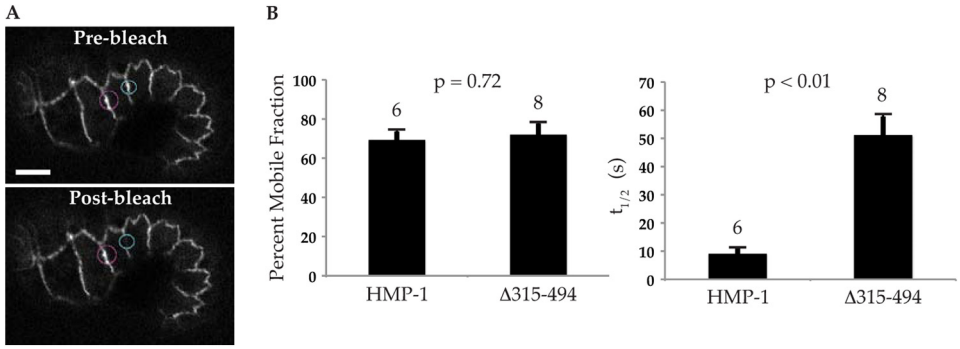

FIGURE 8. **FRAP analysis reveals defects in the rate of recovery for rescuing GFP constructs.** *A,* representative fluorescent confocal images of a homozygous *hmp-1*(*zu278*) mutant embryo rescued by a transgene. The *magenta circle* marks the reference region of interest used in the analysis, whereas the *cyan circle* marks the bleach zone. *Scale bar* = 10 μm. *B*, bar graphs of the average percent mobile fraction and half-life of HMP-1::GFP ($n = 6$) and HMP-1(Δ315–494)::GFP ($n = 8$) in transgenic embryos. *Error bars* indicate S.E., *numbers* indicate *n* value. Although there is no statistically significant difference in the percent mobile fraction for the two transgenes ($p = 0.72$), there is a significant difference in the half-lives as determined by a two-tailed *t* test ($p < 0.01$). Although the transgenes eventually exhibit the same level of recovery, the HMP-1(Δ315–494)::GFP recovers at a much slower rate.

tion to cell-cell contacts and the C-terminal ABD is essential for F-actin recruitment (21). Here we extended this analysis to identify other essential domains and important residues required for HMP-1 function during epidermal morphogenesis. Determining the molecular basis of α-catenin function in a simple metazoan may in turn help to elucidate its functions in higher organisms.

Our analysis of strong LOF *hmp-1* alleles confirms and extends previous studies. Truncation mutants that delete portions of the ABD at amino acids 794, 795, and 826, as well as the missense mutations at 802 and 823, confirm that the C-terminal portion of the ABD is critical for proper F-actin attachment at adherens junctions. We also identified an in-frame deletion (amino acids 687–742) that leaves the rest of the C terminus intact but fails to function *in vivo*. This is the first evidence for a crucial role for the N-terminal-most region of the ABD. Although the available truncation mutants indicate that at least residues 827–927 are important for proper HMP-1 function, our previous *in vitro* work has shown that removal of the nonconserved tail of HMP-1, residues 905–927, from an ABD construct (677–904) has no effect on actin binding in a high speed pelleting assay (21). The novel missense mutation at amino acid 802, in combination with the most C-terminal truncation at 826, suggests that a more discrete region within residues 802–904 may facilitate actin binding in combination with residues 687–742. It is possible that within the tertiary structure of the protein, these two regions form one continuous actin-binding interface. No crystal structures for the C terminus of HMP-1 or αE-catenin have been solved; however, our homology model of the HMP-1 VH3 domain supports this hypothesis, showing that these regions are adjacent (Fig. 6, *A* and *B*). It is also of interest to note that the *hmp-1*(*fe4*) mutation lies within one region, whereas a cluster of intragenic suppressor mutations lies near the other (Fig. 6*C*).

Our homology model also supports another, more speculative possibility that could also explain how regions 802–904 and 687–742 facilitate actin binding. Helices 1 and 2 (Fig. 6*A*), containing residues 687–742, may be one of two discrete F-actin-binding sites, the other comprising residues 802–904. In this case, the full function of HMP-1 would require both sites, not only to allow binding of F-actin, but also bundling. Previous studies have shown the ability of both the N and C termini of αE-catenin to bind F-actin (51), and αE-catenin is known to homodimerize (14, 52, 53), providing two mechanisms for its bundling activity in a full-length protein. We have previously shown, however, that full-length HMP-1 does not form a homodimer *in vitro* (21), making HMP-1 distinct from mammalian αE-catenin, which binds actin more avidly as a homodimer (52). The possibility of dual actin binding sites within the HMP-1 C terminus may explain why HMP-1 does not need to homodimerize. Alternatively, a currently unidentified event may be needed to relieve the intramolecular inhibition observed in full-length HMP-1 *in vivo* (21). Although dual actin binding sites in the tail have been suggested for vinculin (54–56), this mechanism has never been suggested for α-catenin; further experiments would be needed to adequately test this theory.

Recently it has been shown that mammalian vinculin binds to αE-catenin in a force-dependent manner (22). Under low-stress conditions, an inhibitory region of αE-catenin blocks the vinculin-binding site. Upon F-actin binding to the C terminus of αE-catenin and subsequent actomyosin contraction, this inhibitory region is displaced and vinculin is able to bind (22). Subsequent studies in cultured endothelial cells do not support a major role for such tension-dependent vinculin recruitment, however, and even show that the vinculin-binding site of α-catenin is not required for basic adhesion (57). Our studies are the first analysis to address the importance of this conserved domain of α-catenin in an intact organism, and show that HMP-1 residues 315–494 are not necessary for viability. DEB-1/vinculin is not expressed in the epidermis of *C. elegans* (58), which had previously suggested that this domain is not involved in vinculin recruitment in a more simple metazoan. Our results confirm that this domain plays a relatively unimportant role during morphogenesis. It is not clear at this time if the proposed force-dependent regulation of αE-catenin is conserved among the other mammalian isoforms of α-catenin, but it may be that αE-catenin has acquired specializations not found in other vertebrate α-catenins or those of other metazoans.

The domain of αE-catenin that corresponds to amino acids 315–494 of HMP-1 can bind several other actin-related proteins, including α-actinin (15, 29), formin-1 (31), and afadin

(18). Like vinculin, the *C. elegans* homolog of α-actinin, ATN-1, is not expressed in the epidermis (59). There are several formin candidates in *C. elegans*, including FHOD-1, FHOD-2, INFT-1, and FRL-1. Knockdown of each homolog by RNAi does not result in embryonic lethality or body shape defects, and neither does double knockdown of *fhod-2* and *frl-1* (60), suggesting functional redundancy among formins in *C. elegans*. However, *fhod-1*(*RNAi*) was found to enhance the lethality of weak *let-502*/ROCK mutants and suppress the lethality of *mel-11*/myosin phosphatase mutants, two genes with critical functions during embryonic elongation (61–63).[8] *fhod-1*(*RNAi*) does not enhance the penetrance or lethality of *hmp-1(fe4)*,[9] and recent evidence suggests that FHOD-1 is muscle-specific (64). Moreover, the *in vivo* relevance of formin-1 in vertebrates is unclear. Recent evidence in mice suggests that the endogenous protein is not in fact localized to adherens junctions, but instead to the cytoplasm and microtubules (65). Therefore, thus far there is no evidence to suggest that the function of formin-1 depends on HMP-1/α-catenin.

RNAi knockdown of the only afadin homolog in *C. elegans*, *afd-1*, results in very low lethality in a WT background, but enhances the penetrance and lethality of *hmp-1*(*fe4*) to near 100% (45). AFD-1 is also expressed in the epidermis and localizes to cell-cell contacts. However, localization of a significant fraction of AFD-1 depends on the inverted MAGUK protein, MAGI-1, which localizes to a distinct domain basal to the cadherin-catenin complex (46): it is unclear if some AFD-1 physically interacts with HMP-1. In any case, our finding that amino acids 315–494 in HMP-1 are not required suggests that if HMP-1 and AFD-1 interact via this domain, this interaction is quantitatively minor. The ability of this domain in vertebrates to bind other actin-binding proteins may have become more important later in evolution to further stabilize attachment of F-actin to adherens junctions.

Although amino acids 315–494 are not essential, we have shown impaired mobility of HMP-1(Δ315–494)::GFP at the junction compared with full-length HMP-1::GFP. This result suggests that amino acids 315–494 may modulate the efficiency of targeting HMP-1 to sites of cell-cell contact. Although it is possible that deletion of this domain simply causes misfolding of the protein, thereby impeding its mobility, the fact that this construct can completely rescue all lethal developmental defects in *hmp-1*(*zu278*) homozygotes suggests that this is not the case. If amino acids 315–494 do facilitate targeting of HMP-1, our FRAP results indicate that they only affect the rate of deposition of mobile HMP-1, not the overall percentage of mobile protein.

In conclusion, our studies have substantially refined our understanding of the function of conserved residues in the C terminus of α-catenin family members that are required for F-actin binding and epithelial morphogenesis. Our results in turn will allow further focus on the detailed mechanisms by which this key family of proteins links the cadherin complex to the actin cytoskeleton in all metazoans.

[8] P. Mains and C. A. Vanneste, personal communication.
[9] S. L. Maiden, N. Harrison, J. Keegan, B. Cain, A. M. Lynch, J. Pettitt, and J. Hardin, unpublished results.

Acknowledgments—We thank Shoichiro Ono, Bill Bement, Josh Sandquist, and Kevin Sonnemann for helpful discussions regarding experiments, and Jim Priess for providing hmp-1 mutant lines used in this analysis. Some strains were provided by the CGC, which is funded by the National Institutes of Health Office of Research Infrastructure Program Grant P40 OD010440.

REFERENCES

1. Gumbiner, B. M. (1996) Cell adhesion. The molecular basis of tissue architecture and morphogenesis. *Cell* **84,** 345–357
2. Niessen, C. M., Leckband, D., and Yap, A. S. (2011) Tissue organization by cadherin adhesion molecules. Dynamic molecular and cellular mechanisms of morphogenetic regulation. *Physiol. Rev.* **91,** 691–731
3. Benjamin, J. M., and Nelson, W. J. (2008) Bench to bedside and back again. Molecular mechanisms of α-catenin function and roles in tumorigenesis. *Semin. Cancer Biol.* **18,** 53–64
4. Huber, M. A., Kraut, N., and Beug, H. (2005) Molecular requirements for epithelial-mesenchymal transition during tumor progression. *Curr. Opin. Cell Biol.* **17,** 548–558
5. Franke, W. W. (2009) Discovering the molecular components of intercellular junctions. A historical view. *Cold Spring Harbor Perspect. Biol.* 1:a003061
6. Ozawa, M., Baribault, H., and Kemler, R. (1989) The cytoplasmic domain of the cell adhesion molecule uvomorulin associates with three independent proteins structurally related in different species. *EMBO J.* **8,** 1711–1717
7. Reynolds, A. B., Daniel, J., McCrea, P. D., Wheelock, M. J., Wu, J., and Zhang, Z. (1994) Identification of a new catenin. The tyrosine kinase substrate p120cas associates with E-cadherin complexes. *Mol. Cell. Biol.* **14,** 8333–8342
8. Ozawa, M., Ringwald, M., and Kemler, R. (1990) Uvomorulin-catenin complex formation is regulated by a specific domain in the cytoplasmic region of the cell adhesion molecule. *Proc. Natl. Acad. Sci. U.S.A.* **87,** 4246–4250
9. Nagafuchi, A., and Takeichi, M. (1989) Transmembrane control of cadherin-mediated cell adhesion. A 94 kDa protein functionally associated with a specific region of the cytoplasmic domain of E-cadherin. *Cell Regul.* **1,** 37–44
10. Nagafuchi, A., and Takeichi, M. (1988) Cell binding function of E-cadherin is regulated by the cytoplasmic domain. *EMBO J.* **7,** 3679–3684
11. Huber, O., Krohn, M., and Kemler, R. (1997) A specific domain in α-catenin mediates binding to β-catenin or plakoglobin. *J. Cell Sci.* **110,** 1759–1765
12. Aberle, H., Butz, S., Stappert, J., Weissig, H., Kemler, R., and Hoschuetzky, H. (1994) Assembly of the cadherin-catenin complex *in vitro* with recombinant proteins. *J. Cell Sci.* **107,** 3655–3663
13. Pokutta, S., and Weis, W. I. (2000) Structure of the dimerization and β-catenin-binding region of α-catenin. *Mol. Cell* **5,** 533–543
14. Koslov, E. R., Maupin, P., Pradhan, D., Morrow, J. S., and Rimm, D. L. (1997) α-Catenin can form asymmetric homodimeric complexes and/or heterodimeric complexes with β-catenin. *J. Biol. Chem.* **272,** 27301–27306
15. Nieset, J. E., Redfield, A. R., Jin, F., Knudsen, K. A., Johnson, K. R., and Wheelock, M. J. (1997) Characterization of the interactions of α-catenin with α-actinin and β-catenin/plakoglobin. *J. Cell Sci.* **110,** 1013–1022
16. Imamura, Y., Itoh, M., Maeno, Y., Tsukita, S., and Nagafuchi, A. (1999) Functional domains of α-catenin required for the strong state of cadherin-based cell adhesion. *J. Cell Biol.* **144,** 1311–1322
17. Nagafuchi, A., Ishihara, S., and Tsukita, S. (1994) The roles of catenins in the cadherin-mediated cell adhesion. Functional analysis of E-cadherin-α catenin fusion molecules. *J. Cell Biol.* **127,** 235–245
18. Pokutta, S., Drees, F., Takai, Y., Nelson, W. J., and Weis, W. I. (2002) Biochemical and structural definition of the l-afadin- and α-binding sites of α-catenin. *J. Biol. Chem.* **277,** 18868–18874
19. Herrenknecht, K., Ozawa, M., Eckerskorn, C., Lottspeich, F., Lenter, M.,

and Kemler, R. (1991) The uvomorulin-anchorage protein α catenin is a vinculin homologue. *Proc. Natl. Acad. Sci. U.S.A.* **88,** 9156–9160
20. Sarpal, R., Pellikka, M., Patel, R. R., Hui, F. Y., Godt, D., and Tepass, U. (2012) Mutational analysis supports a core role for *Drosophila* α-catenin in adherens junction function. *J. Cell Sci.* **125,** 233–245
21. Kwiatkowski, A. V., Maiden, S. L., Pokutta, S., Choi, H. J., Benjamin, J. M., Lynch, A. M., Nelson, W. J., Weis, W. I., and Hardin, J. (2010) From the cover. *In vitro* and *in vivo* reconstitution of the cadherin-catenin-actin complex from *Caenorhabditis elegans*. *Proc. Natl. Acad. Sci. U.S.A.* **107,** 14591–14596
22. Yonemura, S., Wada, Y., Watanabe, T., Nagafuchi, A., and Shibata, M. (2010) α-Catenin as a tension transducer that induces adherens junction development. *Nat. Cell Biol.* **12,** 533–542
23. Torres, M., Stoykova, A., Huber, O., Chowdhury, K., Bonaldo, P., Mansouri, A., Butz, S., Kemler, R., and Gruss, P. (1997) An αE-catenin gene trap mutation defines its function in preimplantation development. *Proc. Natl. Acad. Sci. U.S.A.* **94,** 901–906
24. Watabe-Uchida, M., Uchida, N., Imamura, Y., Nagafuchi, A., Fujimoto, K., Uemura, T., Vermeulen, S., van Roy, F., Adamson, E. D., and Takeichi, M. (1998) α-Catenin-vinculin interaction functions to organize the apical junctional complex in epithelial cells. *J. Cell Biol.* **142,** 847–857
25. Weiss, E. E., Kroemker, M., Rüdiger, A. H., Jockusch, B. M., and Rüdiger, M. (1998) Vinculin is part of the cadherin-catenin junctional complex. Complex formation between α-catenin and vinculin. *J. Cell Biol.* **141,** 755–764
26. Choi, H. J., Pokutta, S., Cadwell, G. W., Bobkov, A. A., Bankston, L. A., Liddington, R. C., and Weis, W. I. (2012) αE-catenin is an autoinhibited molecule that coactivates vinculin. *Proc. Natl. Acad. Sci. U.S.A.* **109,** 8576–8581
27. Peng, X., Maiers, J. L., Choudhury, D., Craig, S. W., and DeMali, K. A. (2012) α-Catenin uses a novel mechanism to activate vinculin. *J. Biol. Chem.* **287,** 7728–7737
28. Rangarajan, E. S., and Izard, T. (2012) The cytoskeletal protein α-catenin unfurls upon binding to vinculin. *J. Biol. Chem.* **287,** 18492–18499
29. Knudsen, K. A., Soler, A. P., Johnson, K. R., and Wheelock, M. J. (1995) Interaction of α-actinin with the cadherin/catenin cell-cell adhesion complex via α-catenin. *J. Cell Biol.* **130,** 67–77
30. Itoh, M., Nagafuchi, A., Moroi, S., and Tsukita, S. (1997) Involvement of ZO-1 in cadherin-based cell adhesion through its direct binding to α catenin and actin filaments. *J. Cell Biol.* **138,** 181–192
31. Kobielak, A., Pasolli, H. A., and Fuchs, E. (2004) Mammalian formin-1 participates in adherens junctions and polymerization of linear actin cables. *Nat. Cell Biol.* **6,** 21–30
32. Abe, K., and Takeichi, M. (2008) EPLIN mediates linkage of the cadherin catenin complex to F-actin and stabilizes the circumferential actin belt. *Proc. Natl. Acad. Sci. U.S.A.* **105,** 13–19
33. Maiden, S. L., and Hardin, J. (2011) The secret life of α-catenin. Moonlighting in morphogenesis. *J. Cell Biol.* **195,** 543–552
34. Lien, W. H., Klezovitch, O., Fernandez, T. E., Delrow, J., and Vasioukhin, V. (2006) αE-catenin controls cerebral cortical size by regulating the hedgehog signaling pathway. *Science* **311,** 1609–1612
35. Vasioukhin, V., Bauer, C., Degenstein, L., Wise, B., and Fuchs, E. (2001) Hyperproliferation and defects in epithelial polarity upon conditional ablation of α-catenin in skin. *Cell* **104,** 605–617
36. Costa, M., Raich, W., Agbunag, C., Leung, B., Hardin, J., and Priess, J. R. (1998) A putative catenin-cadherin system mediates morphogenesis of the *Caenorhabditis elegans* embryo. *J. Cell Biol.* **141,** 297–308
37. Pettitt, J., Cox, E. A., Broadbent, I. D., Flett, A., and Hardin, J. (2003) The *Caenorhabditis elegans* p120 catenin homologue, JAC-1, modulates cadherin-catenin function during epidermal morphogenesis. *J. Cell Biol.* **162,** 15–22
38. Brenner, S. (1974) The genetics of *Caenorhabditis elegans*. *Genetics* **77,** 71–94
39. Mello, C., and Fire, A. (1995) DNA transformation. *Methods Cell Biol.* **48,** 451–482
40. Ellerbrock, B. R., Coscarelli, E. M., Gurney, M. E., and Geary, T. G. (2004) Screening for presenilin inhibitors using the free-living nematode, *Caenorhabditis elegans*. *J. Biomol. Screen* **9,** 147–152
41. Köppen, M., Simske, J. S., Sims, P. A., Firestein, B. L., Hall, D. H., Radice, A. D., Rongo, C., and Hardin, J. D. (2001) Cooperative regulation of AJM-1 controls junctional integrity in *Caenorhabditis elegans* epithelia. *Nat. Cell Biol.* **3,** 983–991
42. McMahon, L., Legouis, R., Vonesch, J. L., and Labouesse, M. (2001) Assembly of *C. elegans* apical junctions involves positioning and compaction by LET-413 and protein aggregation by the MAGUK protein DLG-1. *J. Cell Sci.* **114,** 2265–2277
43. Zaidel-Bar, R., Joyce, M. J., Lynch, A. M., Witte, K., Audhya, A., and Hardin, J. (2010) The F-BAR domain of SRGP-1 facilitates cell-cell adhesion during *C. elegans* morphogenesis. *J. Cell Biol.* **191,** 761–769
44. Lockwood, C., Zaidel-Bar, R., and Hardin, J. (2008) The *C. elegans* zonula occludens ortholog cooperates with the cadherin complex to recruit actin during morphogenesis. *Curr. Biol.* **18,** 1333–1337
45. Cox-Paulson, E. A., Walck-Shannon, E., Lynch, A. M., Yamashiro, S., Zaidel-Bar, R., Eno, C. C., Ono, S., and Hardin, J. (2012) Tropomodulin protects α-catenin-dependent junctional-actin networks under stress during epithelial morphogenesis. *Curr. Biol.* **22,** 1891–1899
46. Lynch, A. M., Grana, T., Cox-Paulson, E., Couthier, A., Cameron, M., Chin-Sang, I., Pettitt, J., and Hardin, J. (2012) A genome-wide functional screen shows MAGI-1 is an L1CAM-dependent stabilizer of apical junctions in *C. elegans*. *Curr. Biol.* **22,** 1500–1505
47. Pappas, D. J., and Rimm, D. L. (2006) Direct interaction of the C-terminal domain of α-catenin and F-actin is necessary for stabilized cell-cell adhesion. *Cell Commun. Adhes.* **13,** 151–170
48. Arnold, K., Bordoli, L., Kopp, J., and Schwede, T. (2006) The SWISS-MODEL workspace. A web-based environment for protein structure homology modelling. *Bioinformatics* **22,** 195–201
49. Bakolitsa, C., de Pereda, J. M., Bagshaw, C. R., Critchley, D. R., and Liddington, R. C. (1999) Crystal structure of the vinculin tail suggests a pathway for activation. *Cell* **99,** 603–613
50. Rangarajan, E. S., Lee, J. H., Yogesha, S. D., and Izard, T. (2010) A helix replacement mechanism directs metavinculin functions. *PLoS One* **5,** e10679
51. Rimm, D. L., Koslov, E. R., Kebriaei, P., Cianci, C. D., and Morrow, J. S. (1995) α1(E)-catenin is an actin-binding and -bundling protein mediating the attachment of F-actin to the membrane adhesion complex. *Proc. Natl. Acad. Sci. U.S.A.* **92,** 8813–8817
52. Drees, F., Pokutta, S., Yamada, S., Nelson, W. J., and Weis, W. I. (2005) α-Catenin is a molecular switch that binds E-cadherin-β-catenin and regulates actin-filament assembly. *Cell* **123,** 903–915
53. Benjamin, J. M., Kwiatkowski, A. V., Yang, C., Korobova, F., Pokutta, S., Svitkina, T., Weis, W. I., and Nelson, W. J. (2010) αE-catenin regulates actin dynamics independently of cadherin-mediated cell-cell adhesion. *J. Cell Biol.* **189,** 339–352
54. Hüttelmaier, S., Bubeck, P., Rüdiger, M., and Jockusch, B. M. (1997) Characterization of two F-actin-binding and oligomerization sites in the cell-contact protein vinculin. *Eur. J. Biochem.* **247,** 1136–1142
55. Janssen, M. E., Kim, E., Liu, H., Fujimoto, L. M., Bobkov, A., Volkmann, N., and Hanein, D. (2006) Three-dimensional structure of vinculin bound to actin filaments. *Mol. Cell* **21,** 271–281
56. Ziegler, W. H., Liddington, R. C., and Critchley, D. R. (2006) The structure and regulation of vinculin. *Trends Cell Biol.* **16,** 453–460
57. Huveneers, S., Oldenburg, J., Spanjaard, E., van der Krogt, G., Grigoriev, I., Akhmanova, A., Rehmann, H., and de Rooij, J. (2012) Vinculin associates with endothelial VE-cadherin junctions to control force-dependent remodeling. *J. Cell Biol.* **196,** 641–652
58. Barstead, R. J., and Waterston, R. H. (1989) The basal component of the nematode dense-body is vinculin. *J. Biol. Chem.* **264,** 10177–10185
59. Barstead, R. J., Kleiman, L., and Waterston, R. H. (1991) Cloning, sequencing, and mapping of an α-actinin gene from the nematode *Caenorhabditis elegans*. *Cell Motil. Cytoskeleton* **20,** 69–78
60. King, R. S., Maiden, S. L., Hawkins, N. C., Kidd, A. R., 3rd, Kimble, J., Hardin, J., and Walston, T. D. (2009) The N- or C-terminal domains of DSH-2 can activate the *C. elegans* Wnt/β-catenin asymmetry pathway. *Dev. Biol.* **328,** 234–244
61. Piekny, A. J., and Mains, P. E. (2002) Rho-binding kinase (LET-502) and myosin phosphatase (MEL-11) regulate cytokinesis in the early *Caenorh-*

abditis elegans embryo. *J. Cell Sci.* **115,** 2271–2282
62. Piekny, A. J., Wissmann, A., and Mains, P. E. (2000) Embryonic morphogenesis in *Caenorhabditis elegans* integrates the activity of LET-502 Rho-binding kinase, MEL-11 myosin phosphatase, DAF-2 insulin receptor and FEM-2 PP2c phosphatase. *Genetics* **156,** 1671–1689
63. Wissmann, A., Ingles, J., McGhee, J. D., and Mains, P. E. (1997) *Caenorhabditis elegans* LET-502 is related to Rho-binding kinases and human myotonic dystrophy kinase and interacts genetically with a homolog of the regulatory subunit of smooth muscle myosin phosphatase to affect cell shape. *Genes Dev.* **11,** 409–422
64. Mi-Mi, L., Votra, S., Kemphues, K., Bretscher, A., and Pruyne, D. (2012) Z-line formins promote contractile lattice growth and maintenance in striated muscles of *C. elegans*. *J. Cell Biol.* **198,** 87–102
65. Dettenhofer, M., Zhou, F., and Leder, P. (2008) Formin 1-isoform IV deficient cells exhibit defects in cell spreading and focal adhesion formation. *PLoS One* **3,** e2497
66. MacPyMOL (2010) *The PyMOL Molecular Graphics System*, version 1.3, Schrödinger, LLC, Portland, OR

SUPPLEMENTAL EXPERIMENTAL PROCEDURES

Strains - JJ739 (*hmp-1(zu242)/dpy-11(e244)*, *unc-76(e911)* V); JJ743 (*hmp-1(zu244)/dpy-11(e244)*, *unc-76(e911)* V); JJ937 (*hmp-1(zu349)/daf-11(m84ts)*, *sma-1(e30)* V); JJ1172 (*hmp-1(zu402)/daf-11(m84ts)*, *sma-1(e30)* V); JJ1102 (*hmp-1(zu365)/daf-11(m84ts)*, *sma-1(e30)* V); JJ1106 (*hmp-1(zu399)/daf-11(m84ts)*, *sma-1(e30)* V); JJ1191 (*hmp-1(zu404)/daf-11(m84ts)*, *sma-1(e30)* V); JJ1193 (*hmp-1(zu406)/daf-11(m84ts)*, *sma-1(e30)* V); SU401 (+/*nT1(qIs51)* IV; *hmp-1(zu278)/nT1(qIs51)* V; *jcEx110* (pJS434(*hmp-1::gfp*), pRF4(*rol-6(su1006)*))), SU402 (*hmp-1(zu278)/hmp-1(zu278)* V; *jcEx110*), SU407 (+/*nT1(qIs51)* IV; *hmp-1(zu278)/nT1(qIs51)* V; *jcEx113* (pSM10(*hmp-1::gfpΔ315-494*), pRF4(*rol-6(su1006)*))), SU408 (*hmp-1(zu278)/hmp-1(zu278)* V; *jcEx113*), SU409 (+/*nT1(qIs51)* IV; *hmp-1(zu278)/nT1(qIs51)* V; *jcEx114* (pSM13(*hmp-1::gfpΔ710-904*), pRF4(*rol-6(su1006)*))), SU412 (*jcEx116* (pSM5(*hmp-1::gfpΔ194-306*), pRF4(*rol-6(su1006)*)), SU419 (*jcEx123* (pSM21(hmp-*1::gfpΔ13-185*), pRF4(*rol-6(su1006)*)), SU420 (*jcEx124* (pSM17(*hmp-1::gfpΔ13-72*), pRF4(*rol-6(su1006)*)), SU422 (*jcEx126* (pSM15(*hmp-1::gfpΔ504-904*), pRF4(*rol-6(su1006)*)), SU425 (*jcEx130* (pSM2(*hmp-1::gfpΔ315-904*), pRF4(*rol-6(su1006)*)), SU446 (+/*nT1(qIs51)* IV; *hmp-1(zu278)/nT1(qIs51)* V; *jcEx123*), SU449 (+/*nT1(qIs51)* IV; *hmp-1(zu278)/nT1(qIs51)* V; *jcEx124*), SU452 (+/*nT1(qIs51)* IV; *hmp-1(zu278)/nT1(qIs51)* V; *jcEx116*), SU455 (+/*nT1(qIs51)* IV; *hmp-1(zu278)/nT1(qIs51)* V; *jcEx130*), SU462 (+/*nT1(qIs51)* IV; *hmp-1(zu278)/nT1(qIs51)* V; *jcEx126*).

Primers - hmp-*1::gfpΔ13-72* (pSM17), SM23REV (5'-GTTGAAATACGCATGAGAATTGCC-3') and SM4 (5'-CCAATTGCAAACAGTGATCCACGC-3'); *hmp-1::gfpΔ13-185* (pSM21), SM23REV (5'-GTTGAAATACGCATGAGAATTGCC-3') and SM6 (5'-GTTCGACGACGAGCCATTGATTTG-3'); *hmp-1::gfpΔ194-306* (pSM5), SM7REV (5'-CAAATCAATGGCTCGTCGTCGAAC-3') and SM8 (5'-GTTAGTGGTTCTGCTTCAATTGCC-3'); *hmp-1::gfpΔ315-494* (pSM10), SM9REV (5'-GGCAATTGAAGCAGAACCACTAAC-3') and SM10 (5'-GCTCTTGACAATATCACTACTTTGGAC-3'); *hmp-1::gfpΔ315-904* (pSM2), SM9REV (5'-GGCAATTGAAGCAGAACCACTAAC-3') and SM14 (5'-GAGACGGGTCGTGATAGTGACGACGAG-3'); *hmp-1::gfpΔ504-904* (pSM15), SM11REV (5'-GTCCAAAGTAGTGATATTGTCAAGAGC-3') and SM14 (5'-GAGACGGGTCGTGATAGTGACGACGAG-3'); *hmp-1::gfpΔ710-904* (pSM13), SM13REV (5'-GGCAACTTCTCTTTCGAATCGTGTTTG-3') and SM14 (5'-GAGACGGGTCGTGATAGTGACGACGAG-3'); *hmp-1(fe4)*, ES17 (5'-GACTCTGCAATGTTTCTTATTCAAACG-3') and ES18REV (5'-CGTTTGAATAAGAGACATTGCAGAGTC-3'); *hmp-1(fe29)*, ES11 (5'-CCGTCGTCCTAAAGCCAACAGTGTACG-3') and ES12REV (5'-CGTACACTGTTGGCATTAGGACGACGG-3'); *hmp-1(fe27)*, ES9 (5'-GAGTATGACAGAATGCACAAGAGGTTGTGG-3'); hmp1ex1/3S (5'-CTTCTTTATCGTGCGCCTTC-3'); hmp1ex1/3AS (5'-TTGTTCTCACCGTCTCCATC-3); hmp1ex4/5S (5'-AATGACCACCGCGAGTTCAG-3'); hmp1ex4/5AS (5'-GCTTTTACAGCTCGTGGCAC-3'); hmp1ex6-1 (5'-AGCTCTAGACTGAAGCCATG-3'); hmp1ex6-2 (5'-CAGCCGTTATCGTCTGTACG-3'); hmp1ex7-1 (5'-TGCTCGAATGCTTGGAATTC-3'); hmp1ex7-2 (5'-TTATAGAGGGATCCTTGATTC-3'); hmp1ex8-1 (5'-TGTATTCAACGAACGCCGAC-3'); hmp1ex8-2 (5'-CGGGCATATAAAGGATGTGTG-3').

SUPPLEMENTAL FIGURE LEGENDS

SUPPLEMENTAL FIGURE S1. ***Strong loss-of-function (LOF) hmp-1 alleles exhibit morphogenetic failure during embryogenesis.*** (A-AA) Time course of representative wildtype (WT) and homozygous mutant embryos from each allele with DIC microscopy. Anterior is left, dorsal is up. Scale bar is 10 μm. (A-I) WT and homozygous mutants all complete ventral enclosure (0 min). (J-R) WT and mutant embryos elongate to 1.5-fold (55 min), but unlike WT, which continues to elongate to 4-fold (S), the mutants then retract dorsally and exhibit dorsal folds in the epidermis (T-AA, white arrow) indicative of strong zygotic LOF mutants.

SUPPLEMENTAL FIGURE S2. ***Strong LOF hmp-1 mutants are 100% embryonic lethal but exhibit variations in the overall time of death.*** (A) Representative DIC confocal image of a hatchoid (star, no egg shell) next to a dead egg (arrow points to egg shell). Scale bar is 10 μm. Carets denote dorsal humps. "Hatchoid" refers to embryos that have lived long enough to secrete enzymes that degrade the eggshell but eventually die where they were laid. (B) Embryonic lethality counts. Each *hmp-1* allele is maintained as a heterozygote, therefore only 25% of the progeny are expected to be homozygous mutants. The Total Dead includes both Fail to Hatch and Hatchoids. The Total Progeny includes both the Total Dead and the surviving larva. The % Hatchoid is calculated by dividing the Hatchoids by the Total Progeny. The Total % Dead is calculated by dividing the Total Dead by the Total Progeny.

SUPPLEMENTAL FIGURE S3. ***Strong LOF mutations and*** **fe4** ***suppressors occur in highly conserved regions of HMP-1/α-catenin.*** A detailed analysis of the mutations in the C-terminal actin binding domain using a multiple sequence alignment. Unless specified, sequences are of epithelial α-catenin in the species listed. Dark blue = conserved in at least five of the six sequences examined; medium blue = conserved in four of the species examined; light blue = conserved in three of the species examined; white = conserved in two or less species examined.

SUPPLEMENTAL FIGURE S4. ***FRAP indicates amino acids 315-494 aid HMP-1 mobility.*** A co-plot of the point means for fluorescence recovery for HMP-1::GFP (n=6) and HMP-1(Δ315-494)::GFP (n=8). Error bars indicate standard error. Data summarized in Figure 8. Data collected past 100 s for HMP-1(Δ315-494)::GFP is not shown on this graph for consistency with HMP-1::GFP; however, the final percent mobile fraction is accurately indicted in Figure 8.

SUPPLEMENTAL TABLE 1. Strong LOF *hmp-1* alleles

Allele	Amino acid change	Codon change	Strain
zu242	Unknown	Unknown	JJ739
zu244	Δ687-742	Δ2058-2225 bp	JJ743
zu349	Unknown	Unknown	JJ937
zu365	Gln826Ochre	CAA-TAA	JJ1102
zu399	Gln794Amber	CAG-TAG	JJ1106
zu402	Val802Met	GTG-ATG	JJ1172
zu404	Gln433Ochre	CAA-TAA	JJ1191
zu406	Arg187Opal	CGA-TGA	JJ1193

SUPPLEMENTAL TABLE 2. Intragenic suppressors of *hmp-1(fe4)*

Allele	Amino acid change	Codon change	Strain
fe9[1]	Trp861Opal	TGG - TGA	PE113
fe24[1]			PE225
fe26	Arg862Opal	CGA - TGA	PE230
fe13[3]	Thr745Lys	ACA - AAA	PE82
fe22[1]	Gly738Ser	GGT - AGT	PE108
fe25[1]			PE226
fe23	Glu734Lys	GAA – AAA	PE109
fe27	Phe735Cys	TTC – TGC	PE231
fe28	Ala821Thr	TGC - TAC	PE232
fe29[2]	Asn853Lys	AAT - AAA	PE235
fe30[2]	Ala879Val	GCT - GTT	
fe31	Thr736Ile	ACA - ATA	PE236
fe32[3]	Thr745Ile	ACA - ATA	PE245

[1] Independently isolated, identical mutations. [2]These mutations were recovered in the same strain. [3]Same codon affected by independent mutations.

SUPPLEMENTAL FIGURE S1

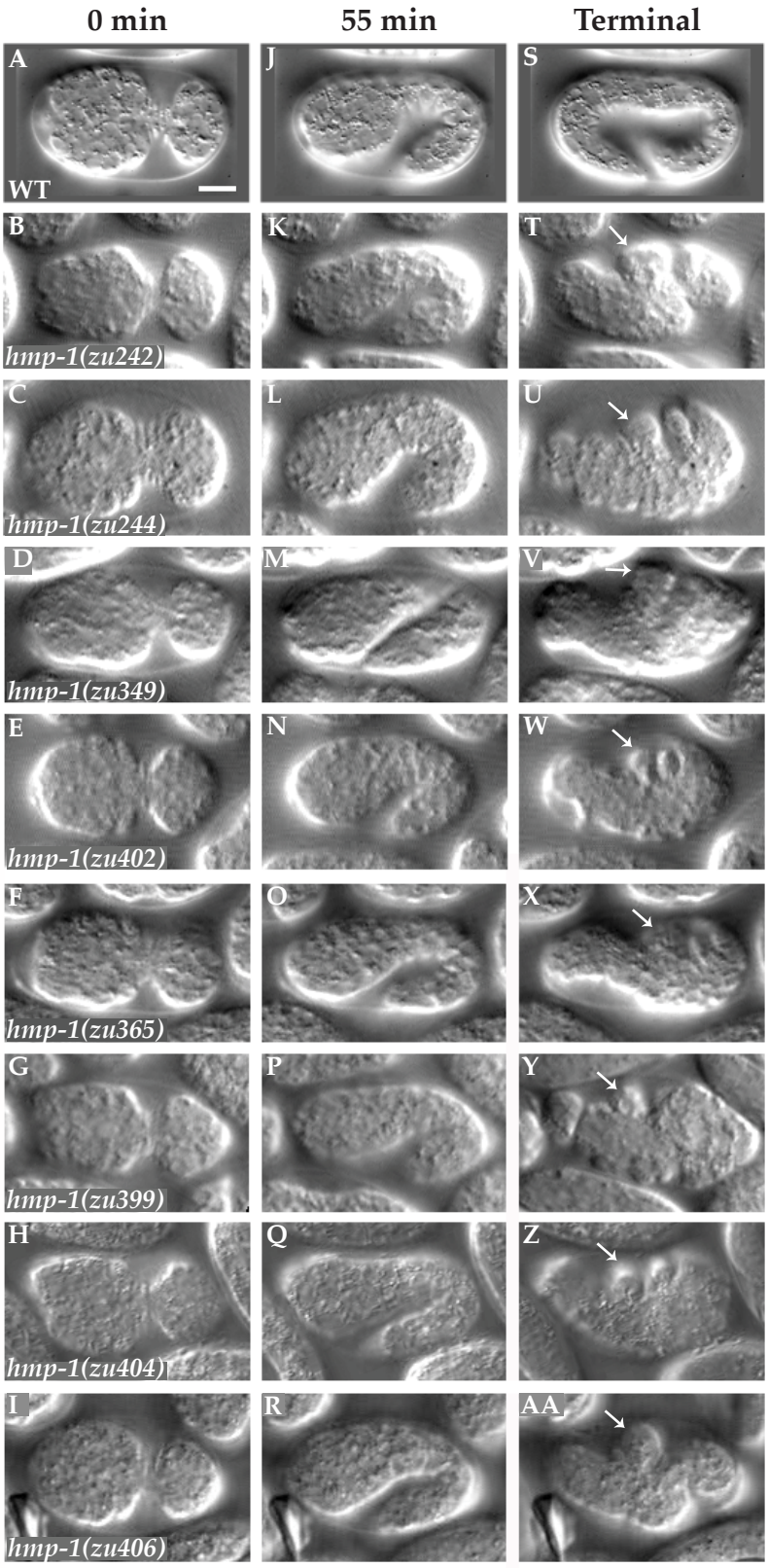

SUPPLEMENTAL FIGURE S2

A

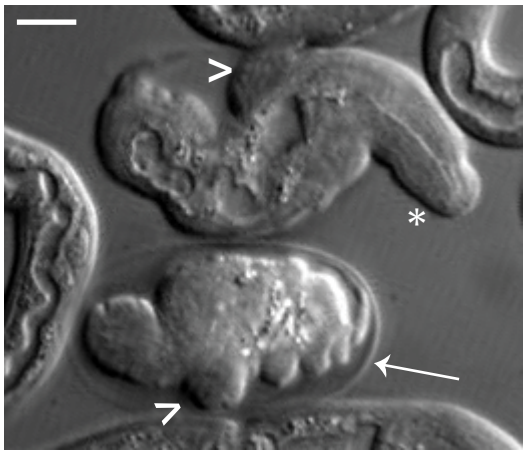

B

hmp-1 Allele	Fail to Hatch	Hatchoids	Total Dead	Total Progeny	% Hatchoid	Total % Dead
zu242	192	0	192	781	0	24.6
zu244	93	94	188	827	11.4	22.7
zu349	38	95	133	545	17.4	24.4
zu402	47	21	68	265	7.92	25.7
zu365	48	30	78	327	9.17	23.9
zu399	46	43	89	360	11.9	24.7
zu404	23	71	94	385	18.4	24.4
zu406	15	66	81	320	20.6	25.3

SUPPLEMENTAL FIGURE S3

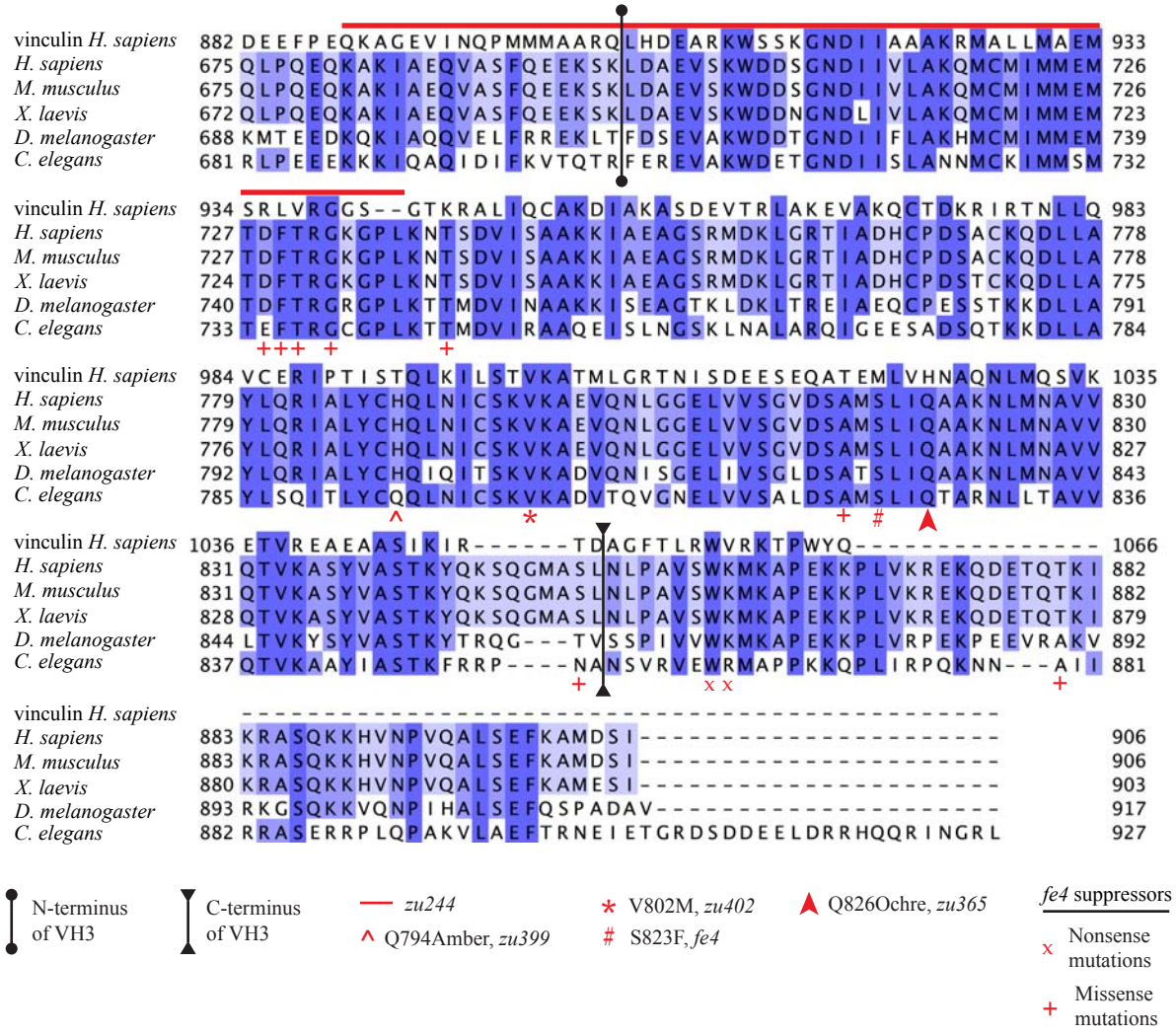

SUPPLEMENTAL FIGURE S4